

Article

Hydroelastic Responses of a Submersible Ring Structure for Offshore Seaweed Cultivation under Wave Action

Huu Phu Nguyen ^{1,*}, Chien Ming Wang ^{1,2}, Brian von Herzen ³ and Chenxuan Huang ¹

¹ School of Civil Engineering, The University of Queensland, St Lucia, QLD 4072, Australia; cm.wang@uq.edu.au (C.M.W.); chenxuan.huang@uq.edu.au (C.H.)

² Blue Economy Cooperative Research Centre, Launceston, TAS 7248, Australia

³ The Climate Foundation, Woodford, QLD 4514, Australia; brian@climatefoundation.org

* Correspondence: huuphu.nguyen@uq.net.au

Abstract: This paper investigates the hydroelastic response of a submersible circular ring structure, designed for offshore seaweed cultivation, under wave action and during the submergence process. The ring structure comprises two circular HDPE pipes connected to each other by equally spaced brackets. The structure carries seaweed grow-out lines, and is kept in position by a mooring-line system used for fish pens. The HDPE collar is equipped with multiple inlet and outlet valves, allowing it to be submerged to avoid strong waves and to be raised to the water surface when the strong waves die down. The software AquaSim was used for the hydroelastic analysis of the moored structure. It is found that we can significantly reduce the von Mises stresses in the ring structure as well as the mooring-line forces by submerging. However, the structure can experience significant increase in stress during the submergence process due to bending from combined wave action and non-uniform distribution of filled water in the ring structure. This stress increase may cause structural damage or even failure. Therefore, it is important to submerge the ring structure in calm waves ahead of predicted storms and to control the distribution of seawater into the ring structure. For the latter, it is best to use at least two inlet valves and two outlet valves to minimize the likelihood of damage of the ring structure during the submergence process.

Keywords: hydroelastic responses; submersible ring structure; seaweed cultivation



Citation: Nguyen, H.P.; Wang, C.M.; von Herzen, B.; Huang, C.

Hydroelastic Responses of a Submersible Ring Structure for Offshore Seaweed Cultivation under Wave Action. *J. Mar. Sci. Eng.* **2023**, *11*, 2238. <https://doi.org/10.3390/jmse11122238>

Academic Editor: Spyros A. Mavrakos

Received: 31 October 2023

Revised: 20 November 2023

Accepted: 23 November 2023

Published: 27 November 2023



Copyright: © 2023 by the authors. Licensee MDPI, Basel, Switzerland. This article is an open access article distributed under the terms and conditions of the Creative Commons Attribution (CC BY) license (<https://creativecommons.org/licenses/by/4.0/>).

1. Introduction

Seaweed, also known as marine macroalgae, is an amazing natural resource with wide-ranging applications such as food, pharmaceutical and biomedical products, biodegradable plastics, textiles, and packaging materials [1–3]. It is no wonder that the global seaweed industry is the fastest growing component of global food production, and has been increasing by about 10% per year since 2010, reaching USD 15 billion in 2019 [1–3]. Greater than 90% of global seaweed production comes from East Asia [1].

Most common farming methods of seaweed involve using ropes and nets in nearshore sheltered waters, where seaweeds are attached to ropes or nets that are kept below the water surface by wooden piles, plastic buoys, floating bamboo frames and seabed anchors [4]. These common farming methods have the advantages of low costs due to the simple farming infrastructure and easy installation, operation, and harvesting. However, nearshore seaweed farms are facing several problems: (i) competition with other coastal developments such as tourism, fishing, shipping, and floating urban developments; (ii) the rising temperature of coastal shallow waters that retards the growth of seaweed; and (iii) increasing environmental risks due to seaweed harbouring parasites and diseases, and slowing water flows in coastal regions [1]. For increasing seaweed production and solving the existing challenges to nearshore seaweed farming, the Food and Agriculture Organization [1] and the research community [5–7] have identified moving to offshore locations as a viable strategy for large-scale seaweed farming. This strategy is already being considered for large-scale sustainable

fish farming [8]. Offshore sites offer several advantages: (i) the vast expanse of open sea permits large-scale seaweed aquaculture; (ii) seaweed platforms can be positioned at optimal depths to ensure sufficient sunlight and temperature for maximal growth; (iii) potential environmental risks can be minimized, and (iv) cooler temperatures [6].

A key challenge in offshore seaweed cultivation is for the infrastructure and seaweed to survive in highly energetic environments, especially during severe storms. This has spurred researchers and engineers to devise specialized infrastructure for offshore seaweed cultivation. Initial efforts in this direction can be traced back to the 1970s in the United States. During this time, an innovative floating structure resembling an inverted umbrella was designed and tested. It features a central buoy and upwelling pipes to bring cold water rich in nutrients to irrigate the seaweed for accelerated growth [9]. Other earlier infrastructure concepts include the 2010 seaweed carrier proposal from Norway, the deployment of a tension-leg platform system in South Korea in 2016, the BioArchitecture Lab system in Chile in 2010, and the Macroalgal Cultivation Rig in the Faroe Islands between 2010 and 2019 [5]. Designs relying on buoys, lines, and anchors (such as those by the BioArchitecture Lab and the Macroalgal Cultivation Rig) have demonstrated comparably lower capital and operational expenses (CAPEX and OPEX) when contrasted with those involving floating steel frames like the inverted umbrella structure and the tension-leg platform system [5]. However, it is important to note that such buoy–line–anchor systems have yet to reach the commercialization stage. The ongoing USD 55-million MARINER and UNITED programs in US and Europe [10,11] are attempting to further improve seaweed-cultivation infrastructure designs. Some ideas that have been investigated in these programs include the use of a single-point mooring system, submerging seaweed infrastructure, and optimizing the configuration of buoy–line–anchor systems.

The ongoing development and global interest in offshore seaweed-cultivation infrastructure have certainly created a need for R&D in obtaining engineering knowledge and techniques for safe and cost-effective infrastructure designs. This need is critical if we are going to farm seaweed offshore, as we have witnessed structural failures in trial deployments of the upside-down-umbrella-like structure, and SPAR buoys and H-frames [5]. Unfortunately, research in this area is rather limited. Some recent studies [12,13] have focused on understanding wave attenuation and the hydrodynamics of kelp by conducting model tests of one or several lines of artificial seaweeds under wave/current action. However, there is little study on the hydrodynamics of entire floating seaweed infrastructure including buoys, seaweed lines, mooring lines, anchors, and other supporting structures. Nguyen et al. [14] recently reported a preliminary study on the hydroelastic analysis of a submersible circular seaweed platform in floating and submerged states. The ability of the seaweed platform to submerge to an appropriate water depth is essential for offshore seaweed-cultivation infrastructure and for the seaweed to survive during severe storms.

The present study extends the earlier study [14] to investigate hydroelastic responses of offshore seaweed ring structures in not only the floating and submerged states, but also during the submergence process. Hydroelastic analysis is needed because of the employment of a flexible high-density polyethylene (HDPE) ring structure to carry the seaweed grow-out lines. The flexibility of the HDPE ring structure under wave action results in its dynamic response being primarily governed by elastic deformations, as opposed to rigid body motions. More details on hydroelastic analysis can be found in the following references [15–20]. HDPE has been selected as the primary structural material for the ring structure due to its durability in harsh sea environmental conditions, high resistance to corrosion and UV light, good antibiofouling properties and its being easy to fabricate into any shape [21,22]. The HDPE circular ring structure is widely employed as floating collars for open-net fish pens. Constructing HDPE ring structures for seaweed cultivation can be done by utilizing current fabrication methods and repurposing disused HDPE pipes from fish farms, offering improved waste management and cost savings. HDPE pipes, mats and connector systems are also being adopted for fish pens, e.g., Marine Donut [23] and the SeaFisher [24]. In the next sections of this paper, we will introduce conceptual

designs of seaweed infrastructure systems. Subsequently, hydroelastic analysis of the infrastructure designs by using AquaSim will be presented. The hydroelastic responses of the HDPE ring structure and the forces in mooring lines will be examined at various stages of submergence.

2. Design of Seaweed Infrastructure

Consider a floating ring structure made from two circular HDPE pipes held together by equally spaced brackets. The ring structure supports seaweed grow-out lines and is kept in position by a mooring-line system as shown in Figure 1. The mooring-line system follows that of the conventional open-net fish cages. Such a conceptual design can be used for farming red seaweeds (such as *Gracilaria dura*, *Kappahycus alvarezii* and *Eucheuma*). Young seaweed is placed inside tube nets for better protection from strong environmental actions in offshore sites. The tube nets are attached to the seaweed grow-out lines. Examples of seaweed tube nets can be found in [25].

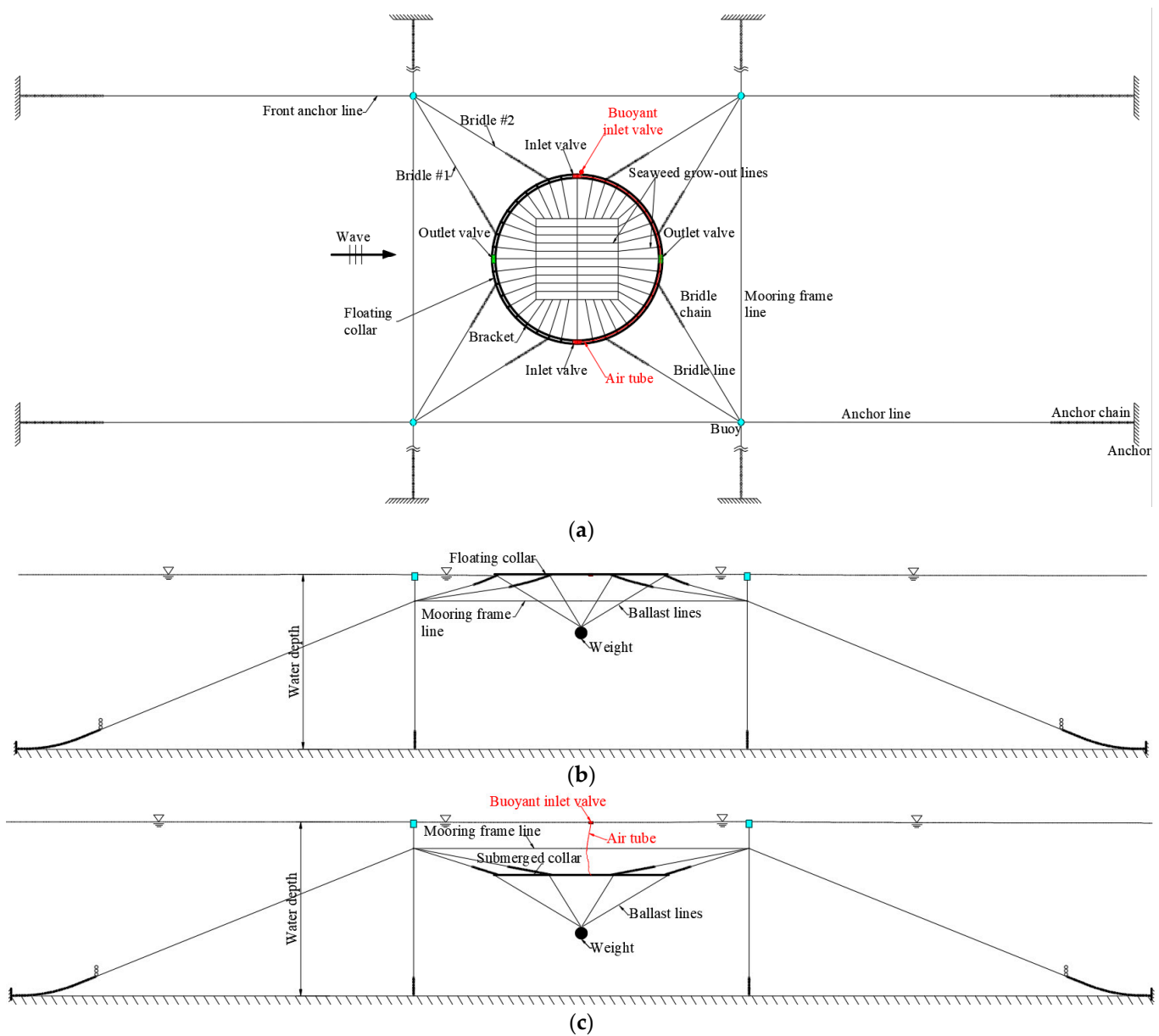


Figure 1. Submersible seaweed platform with concentrated ballast weight: (a) plan view, (b) side view of floating state, (c) side view of submerged state.

Seaweed lines/tube nets are arranged as shown in Figure 1a. This arrangement allows for the maximum number of seaweed tube nets within the enclosed sea space. An exclusively radial alignment of seaweed lines would be suboptimal, as it would result in a concentrated density of seaweed at the central section. The diameter of the initial seeded tube nets is taken as 10 cm based on the typical arrangement of tube nets used for farming red seaweed [25]. The spacing between seaweed tube nets is about 1.2 m, as per the recommendation from Ref. [26]. An adequate spacing between the tube nets is necessary to allow all the seaweed to get sunlight and nutrients as well as to reduce entanglement of the seaweed.

The side elevation of the floating seaweed platform is shown in Figure 1b. The HDPE ring structure carries sidewalks for workers to safely access the floating seaweed structure from support vessels that are berthed alongside. The ring structure has either one or two inlet valves placed directly opposite to each other, and one or two outlet valves. The seawater enters the HDPE pipes through the inlet valves, while the air escapes through the outlet valves during the submergence operation. To refloat the ring structure, compressed air from an air compressor unit in a vessel is pumped into the inlet valves while the seawater is forced out through the outlet valves. Air tubes are used to transmit the compressed air from the buoyant air valve to the inlet valves. Upon reaching the desired water depth, the submerged ring structure is suspended by a system of duck diving buoys and lines as shown in Figure 1c. This technology for submerging the structure has been developed and tested in the fish farming industry (see [27] as an example).

Note that, as the mass density of HDPE is smaller than that of seawater, we need to add ballast weights to the HDPE ring structure so as the structure can be submerged when filled with water. We considered two different ballast weight systems. One system makes use of a concentrated weight attached to the ring structure by lines as shown in Figure 1b,c. The other system makes use of multiple weights that are attached to the HDPE ring structure as shown in Figure 2. In shallower waters, the multiple-weights system allows the ring structure to be submerged closer to the seabed for maximum protection from the strong surface waves in storm events. In the concentrated-weight system, the ring structure can only be submerged to the point where the weight rests on the seabed. For the least amount of line materials, the lines holding the concentrated weight should be 45 degrees with respect to the vertical position (see [28] for the proof).

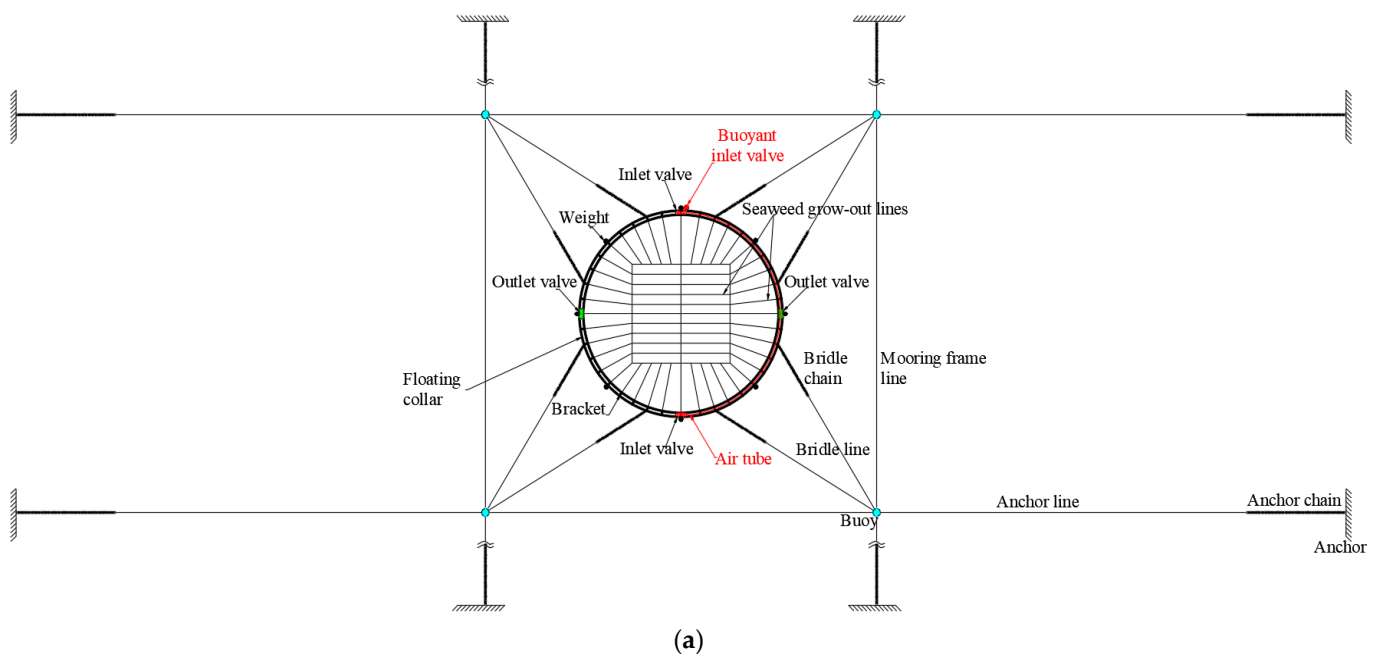


Figure 2. Cont.

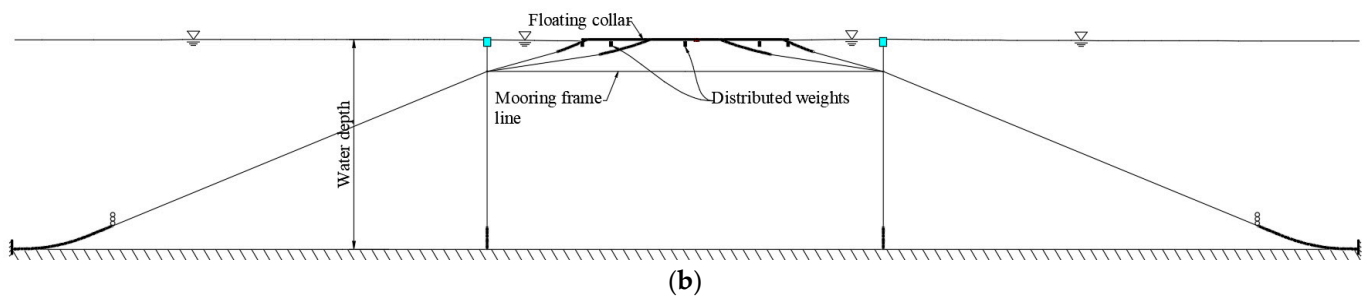


Figure 2. Seaweed platform with distributed ballast weights: (a) plan view, (b) side view.

The mooring-line arrangement, as illustrated in Figure 1 and proven successful in fish-farming applications, keeps the ring structure in place. The mooring lines consist of chains and wire ropes, where the chains offer weight and a catenary influence, and the wire ropes offer enhanced elasticity and lower costs per unit length [29]. Typically, a mixed mooring line of chains and wire ropes is favoured. Chains are employed to connect the wire ropes to the anchor points and also the ring structure to the wire ropes, as shown in Figure 1a, to increase the holding power and provide resistance to abrasion [30]. The chains are then anchored to the seabed by plate anchors.

In the considered floating seaweed-cultivation infrastructure, we utilize sizes for collars, mooring setups, and buoys that are employed in floating open-net fish cages [31]. The design characteristics of the seaweed-cultivation infrastructure are given in Table 1. The sea-state conditions considered are presented in Table 2. Regular waves are assumed. Note that the sea state S3 is rather severe, and is the measured extreme condition in Storm Bay, Tasmania, Australia where offshore aquaculture is considered [24].

Table 1. Design parameters of seaweed platform.

Components	Description	Magnitude	Unit
Ring structure	Diameter of outer circular HDPE pipe	51.8	m
	Diameter of inner circular HDPE pipe	50	m
	Number of brackets	60	-
	Tube section diameter	0.45	m
	Tube bending rigidity	7.72×10^5	Nm ²
Bridle Line/chain	Tube mass	32.54	kg/m
	Line diameter	0.04	m
	Line stiffness	486.1	kN/m
	Chain diameter	0.0224	m
	Chain length	5.47	m
Frame line	Chain mass	8.66	kg/m
	Line length	100	m
	Line depth	8	m
	Line diameter	0.0512	m
	Line stiffness	1.03×10^3	kN/m
Anchor line	Line length	103.5	m
	Line diameter	0.0512	m
	Anchor line stiffness	110.2	kN/m
	Anchor chain length	30	m
	Anchor chain diameter	0.032	m
Ballast lines	Anchor chain mass	16	kg/m
	Line length	70	m
	Line diameter	0.04	m
Buoy	Line stiffness	486.1	kN/m
	Buoy diameter	1.55	m
	Buoy length	2.34	m

Table 1. *Cont.*

Components	Description	Magnitude	Unit
Tube nets	Diameter of tube nets	10	cm
	Spacing between tube nets	~1.2	m
	Submergence depth	16	m
	Weight	3000	kg

Table 2. Sea state conditions considered for analysis of seaweed ring structure.

Sea State Conditions	Wave Height H (m)	Wave Period T (s)
S1	2.5	6
S2	4	8
S3	8	12

3. Methodology

We shall first introduce models for the ring structure and mooring systems, which have undergone rigorous development and validation processes in fish-cage analysis [31]. Subsequently, we shall discuss a modelling approach for seaweed nets in waves. The hydroelastic analysis of the seaweed-cultivation infrastructure will be carried out by using the AquaSim software version 2.18 [32].

3.1. Modelling of the Ring Structure and Mooring-Line Systems

In accordance with the established modelling conventions in fish-cage analysis, the ring structure (comprising two HDPE circular pipes held together by 60 HDPE brackets) is modelled by beam elements, while the mooring lines/chains are modelled by truss elements. The buoys are modelled by spring elements. The spring stiffness is determined from the buoy’s geometry. Furthermore, our modelling framework assumes that the material constitutive relations governing the ring structure and mooring lines obey Hooke’s law. The AquaSim software is used for the hydroelastic analysis. AquaSim makes use of the Finite Element (FE) method and allows for geometric nonlinearities due to large translations and rotations of the flexible ring structure. It considers hydrodynamic (diffraction) forces as well as Morison loads from wave and current. The Morison loads include hydrodynamic forces such as drag force and Froude–Krylov diffraction force and added mass. Therefore, the hydroelastic interactions between the fluid and the flexible structure at the surface state as well as at submerged states at various water depths can be investigated within AquaSim. For the hydroelastic simulations, the drag and mass coefficients are assumed to be 1 and 2, respectively. These values are chosen based on the findings from numerical and experimental studies conducted on HDPE floating fish cages [31].

3.2. Modelling of Seaweed Tube Nets

Red seaweeds are cultivated within cylindrical nets that provide protection against harsh wave forces. Examples of such red-seaweed “tube nets” are shown in [25], and in Figure 3. In the numerical simulations, the seaweed cylindrical nets are modelled as permeable cylindrical membranes, where the membrane porosity is calibrated from physical tests either in a hydraulics laboratory or in the field. This porosity is contingent upon parameters including seaweed morphology, dimensions, and biomass density. In addition, it is important to note that red seaweeds grow over time and are harvested typically within 40–75 days [33]. The development of a model for red-seaweed tube nets is thus rather challenging. Here, we adopt a rational modelling approach where the membrane’s porosity is assumed to be 1 (i.e., impermeable tube). This is believed to be the worst scenario in terms of wave/current loads on the tube net and thus will provide a conservative design for the seaweed ring structure and mooring lines. It is evidenced from the literature [34,35] that environmental loads on perforated cylinders are smaller than those on impermeable

cylinders. The initial tube nets used for seeding have a diameter of 75 mm, whereas the tube nets containing mature seaweed ready for harvesting measure approximately 200 mm–300 mm in diameter [25]. In the numerical model of this study, seaweed tube nets are modelled as 20-cm diameter impermeable tubes. The tube mass density is defined to be equivalent to the mass density of the seaweeds which are approximately equal to the water mass density [36]. The wave/current loads acting on seaweed lines are estimated by using the Morison equation.

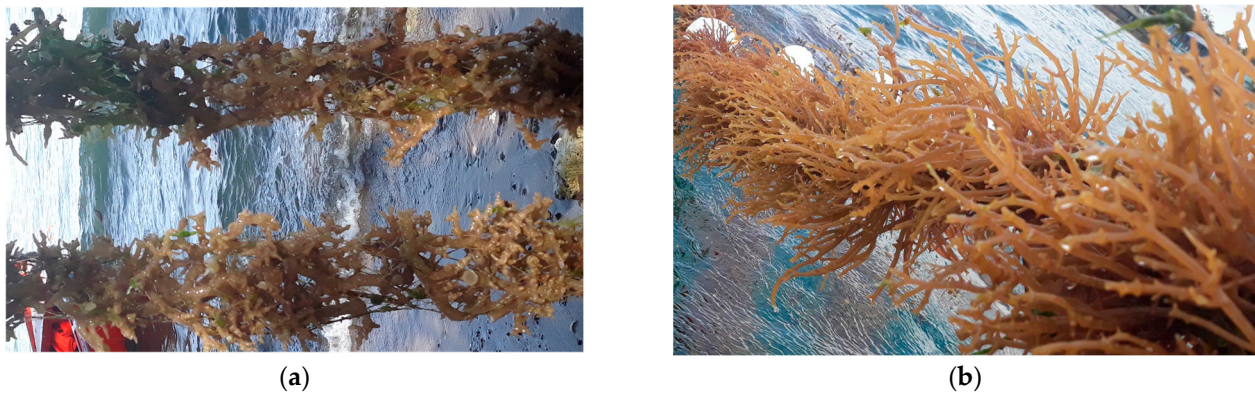


Figure 3. (a) Tube nets with young seaweed (*Kappaphycus alvarezii*), and (b) tube nets with mature seaweed. Photos courtesy of The Climate Foundation.

4. Numerical Examples

4.1. Hydroelastic Responses of the Ring Structure in a Floating State

In this section, we investigate mooring forces in the front anchor line, and bridle lines #1 and #2, as well as the displacements and von Mises stresses at nine points as shown in Figure 4. Figure 5 presents mooring forces when using either a concentrated ballast weight or a distributed ballast weight. The mooring forces for the ring structure with a concentrated weight are rather close to those obtained for the ring structure with a distributed weight for sea states S1 and S2. However, for the severe sea-state condition S3, the use of a concentrated weight results in smaller mooring forces.

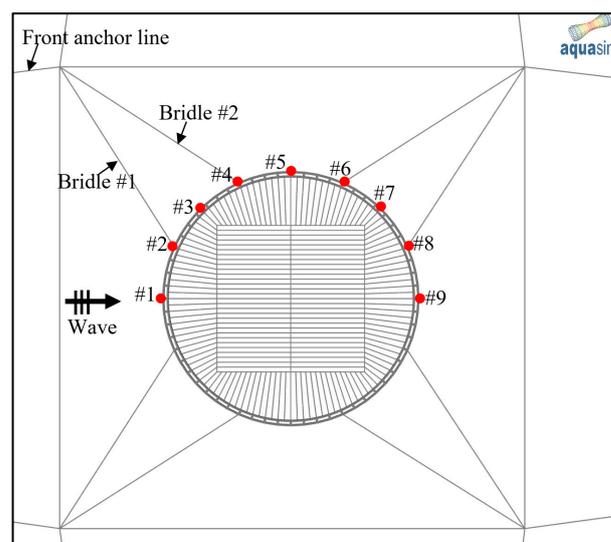


Figure 4. Locations for measuring von Mises stresses and displacements.

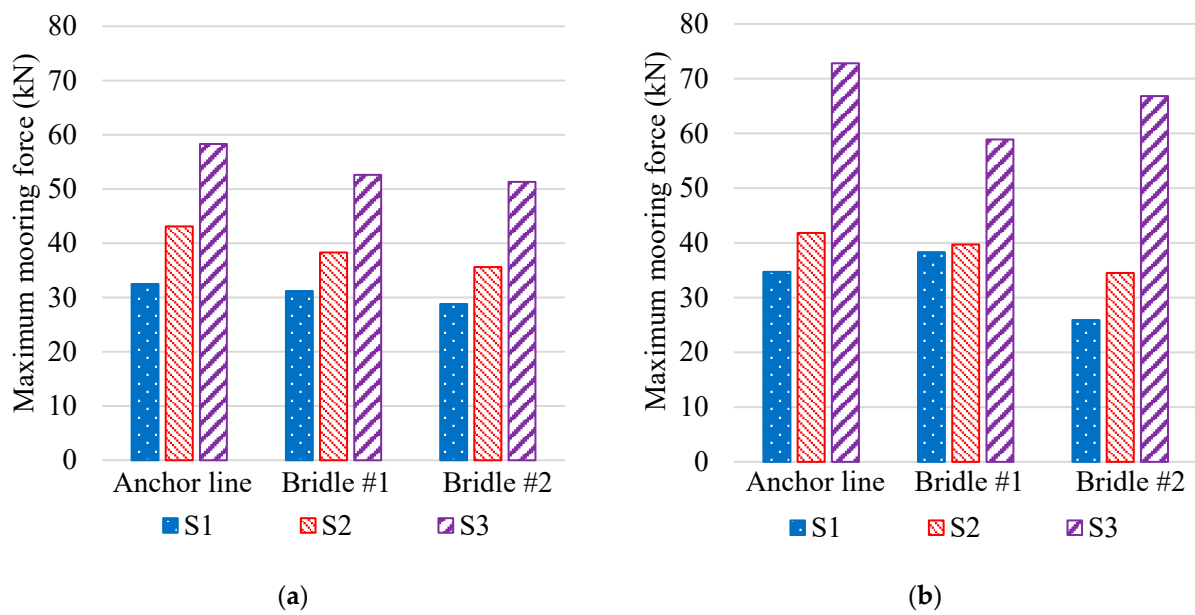


Figure 5. Maximum mooring forces in front anchor line, bridle line #1, and bridle line #2: (a) for concentrated ballast weight, (b) for distributed ballast weights.

The mooring forces in the severe sea-state condition S3 are clearly significantly higher than the mooring forces in the more benign sea-state conditions S1 and S2. For example, for the ring structure with a distributed weight, the tension in the front anchor line in sea state S3 is about 100% larger than that in sea state S1.

Figure 6 presents maximum total displacements of the ring structure at various locations of the HDPE collar for sea-state conditions S1, S2, and S3. Here, the total displacement w is defined as $w = \sqrt{w_x^2 + w_y^2 + w_z^2}$ where w_x , w_y , and w_z are displacement components along the x -, y -, and z -axes, respectively. The results clearly show that the maximum displacements increase from sea states S1 to S3 due to the increase in the incident wave height. Figure 7 presents maximum von Mises stresses in the ring structure at various locations for sea-state conditions S1, S2 and S3. The maximum stresses are located at the connections with the bridle lines. Although the force in bridle #1 may be larger than the force in bridle #2 (Figure 5), the stress at the bridle #1 connection with the collar (at location #2 in Figure 4) may be smaller than that at the bridle #2 connection with the collar (at location #4 in Figure 4). This is because the vertical component of wave forces causes bending stress in the collar, but it should not significantly change the forces in the bridle lines which are used to mainly restrain horizontal motions of the collar. The maximum stresses may be reduced by introducing an additional bridle line between bridle #1 and bridle #2. As expected, the stresses are largest at sea state S3, where the maximum stress can exceed 10 MPa. Submergence of the ring support is needed to reduce the stress levels. For the other sea-state conditions S1 and S2, the stress is below 8 MPa. Figure 8 shows the distributions of displacements and stresses in the ring structure at the water surface for the different sea states S1, S2 and S3. It can be seen that the ring structure deforms considerably from its original circular shape to a distorted circular shape, with the most distortion for sea state S3.

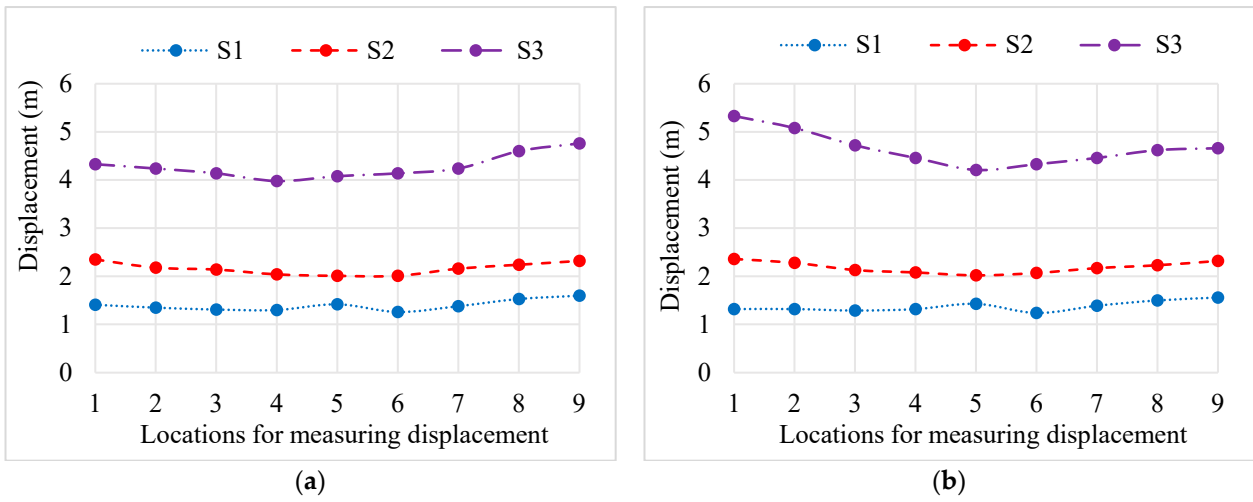


Figure 6. Maximum displacements at various locations of HDPE collar for S1–S3: (a) for concentrated ballast weight, (b) for distributed ballast weights.

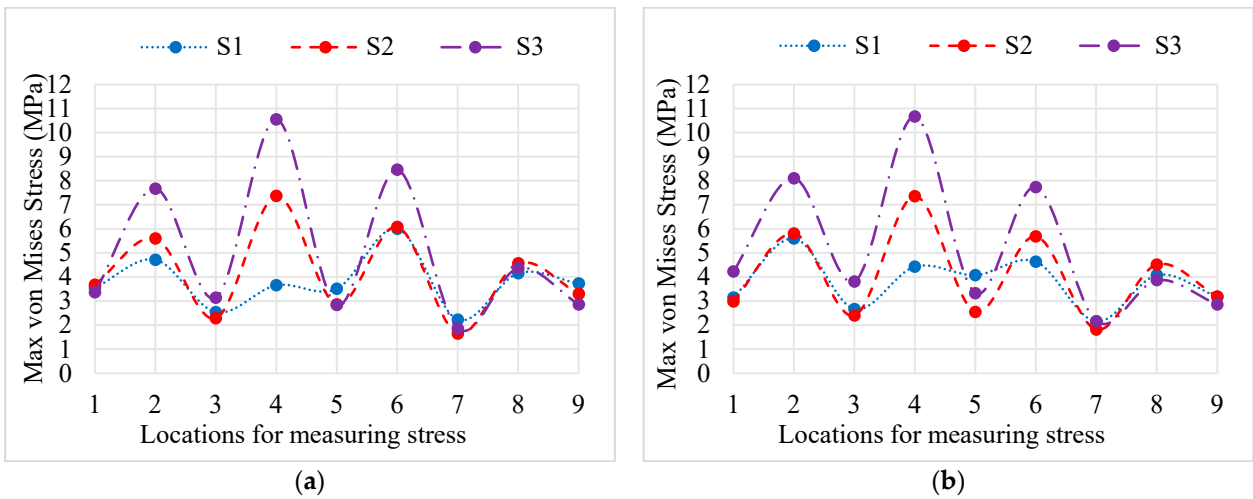
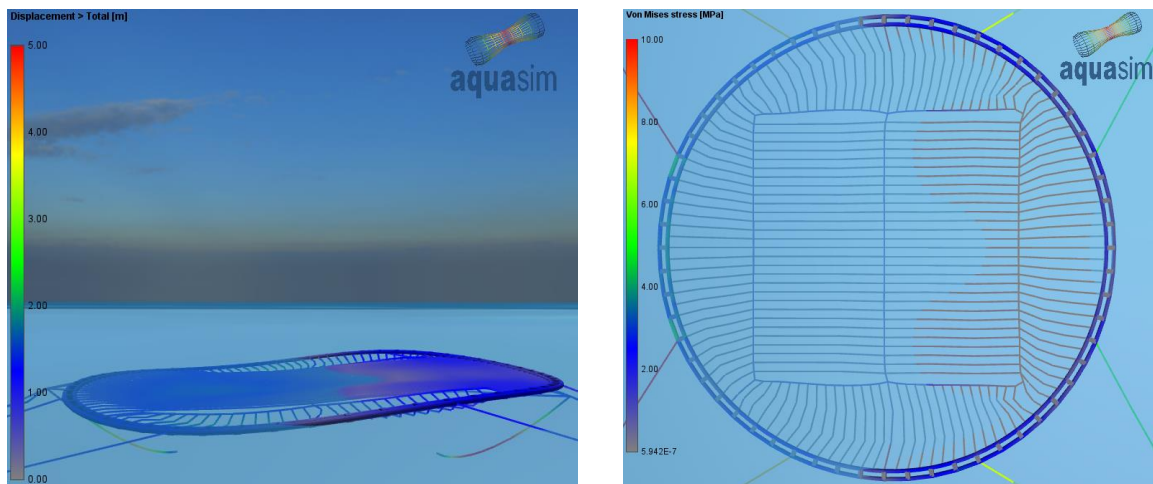


Figure 7. Maximum von Mises stresses at various locations of HDPE collar for S1–S3: (a) for concentrated ballast weight, (b) for distributed ballast weights.



(a)

Figure 8. Cont.

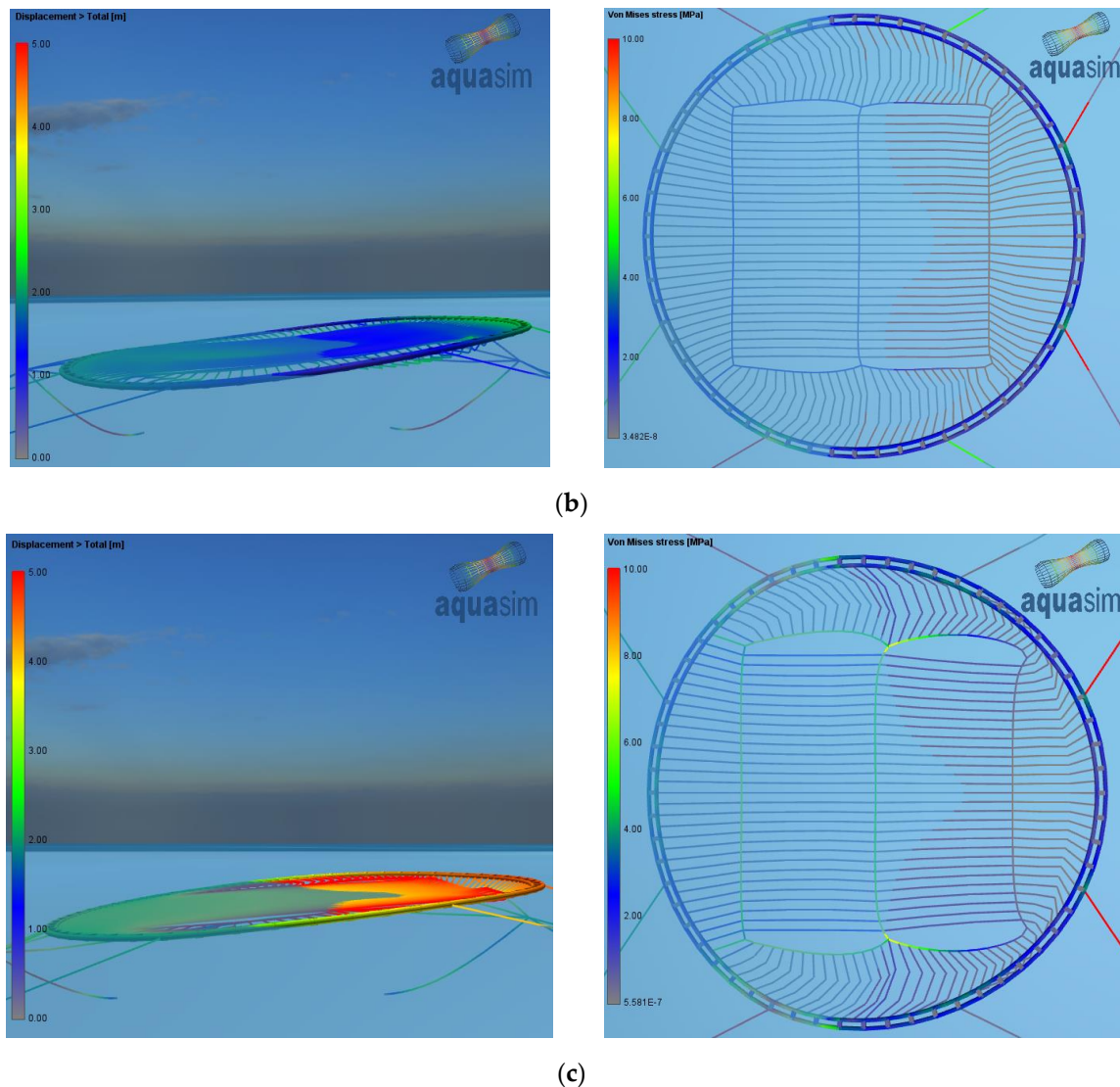


Figure 8. Displacements and von Mises stress distributions in HDPE ring structure for sea states: (a) S1, $t = 9$ s, (b) S2, $t = 12$ s, (c) S3, $t = 16$ s where t indicates the time in AquaSim simulations.

4.2. Hydroelastic Responses of the Ring Structure at Different Submergence Stages

This section aims to: (i) investigate the reductions in mooring forces and stresses in the ring structure when it is fully submerged; and (ii) investigate the effects of using either one or two inlet and outlet valves on the stresses of the ring structure during the submergence procedure.

4.2.1. At Floating and Fully Submerged States

We shall compare the hydroelastic responses of the ring structure at the water surface and at the fully submerged state where the ring is 16 m below the water surface. The distributed ballast weight system is adopted in this investigation.

Figure 9 presents tensile forces in the front anchor line, bridle line #1, and bridle line #2 in floating and submerged states for sea state S3. It can be seen that, when the whole ring structure is filled with water and is fully submerged at a depth of 16 m, the mooring forces are reduced significantly. For sea-state condition S3, the tension in the front anchor line is reduced by about 50% by submerging the collar completely. The significant reduction in mooring forces shows an increase in survivability of the mooring-line systems in storm events via submerging the ring structure to dodge the strong surface waves.

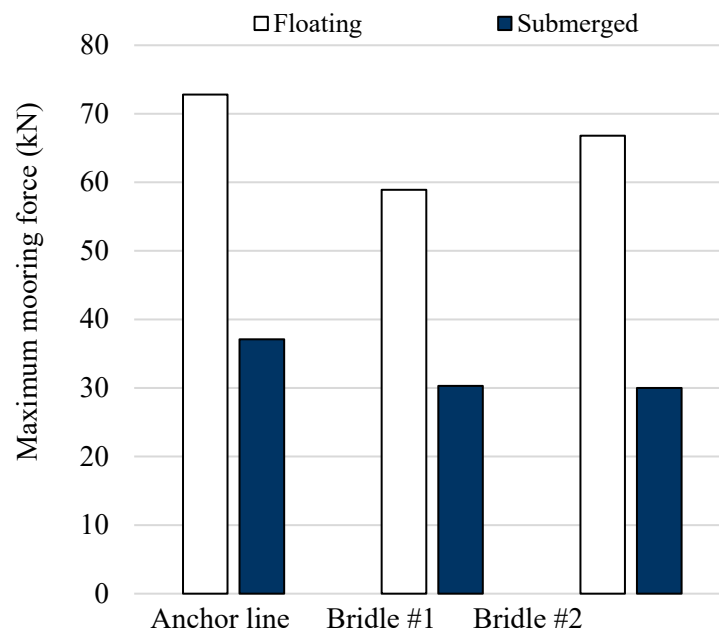


Figure 9. Mooring forces in anchor line, bridle lines #1 and #2 for sea state S3.

Figure 10 presents maximum von Mises stresses in the ring structure at the nine locations for sea-state condition S3. The maximum stresses are found at the connections with the bridle lines as expected. It can be seen that the stresses can be reduced by about 50% by filling the whole ring structure with water, and letting it sink to 16 m below the water surface.

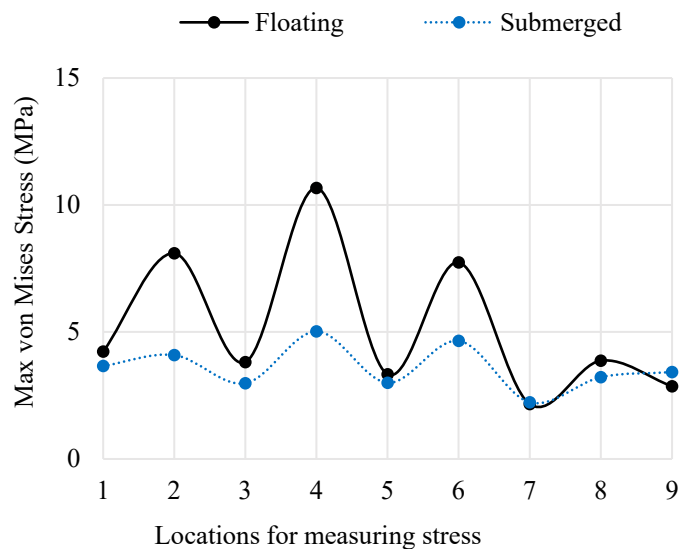


Figure 10. Variations of maximum von Mises stresses in ring structure at water surface and at 16 m below water surface for sea state S3.

4.2.2. Effects of Valve Configuration

Locations and numbers of valves need to be determined as part of the submergence strategy. This section investigates the effects of using either one or two inlet and outlet waves located in the ring structure on hydroelastic responses of the ring structure. Consider two valve configurations C1 and C2 as shown in Figures 11 and 12. The red circles show the locations of inlet valves, whereas the green circles show the locations of outlet valves. Valve configuration C1 has been adopted in submersible fish cages designed by Badinotti [27], whereas valve configuration C2 has been used in the submersible fish-cage design by

Aquatec [37]. For each valve configuration, the responses of the ring structure are determined for five submergence stages, defined by the percentage of the ring structure filled with seawater, as shown in Figures 11 and 12 (from left to right). Stage 1 is the ring structure filled with air (i.e., 0% of seawater). Stage 2 represents 25% of the ring structure filled with water, Stage 3 represents 50% of the ring structure filled with water, State 4 represents 75% of the ring structure filled with water, and Stage 5 represents 100% of the ring structure filled with water.

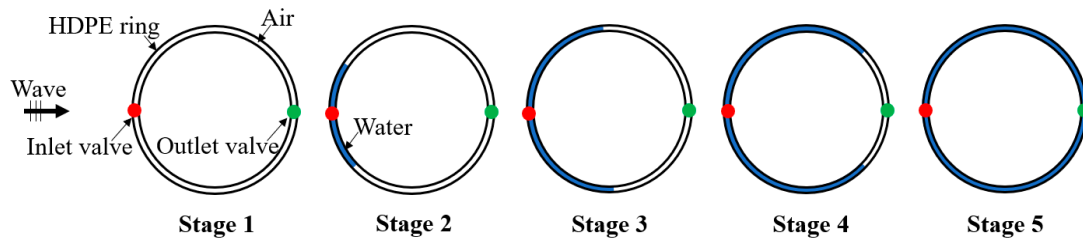


Figure 11. Top views of five submergence stages for ring structure with 1 inlet valve and 1 outlet valve denoted as valve configuration C1.

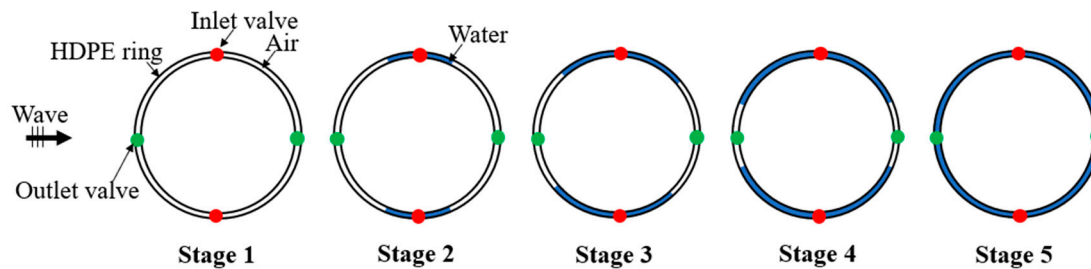


Figure 12. Top views of five submergence stages for ring structure with 2 inlet valves and 2 outlet valves denoted as valve configuration C2.

Figure 13 shows the von Mises stresses in the ring structure with different configurations of valves at Stages 2, 3 and 4 in calm waters (i.e., the wave height is very small). Note that the stresses in Stage 1 and Stage 5 are not shown in Figure 13 as they are negligible in calm waters. It can be seen from Figure 13 that the stress in the ring structure is affected significantly by the configuration of inlet and outlet valves. For valve configuration C1, the von Mises stress can reach 4.2 MPa. For valve configuration C2 with two inlet valves and two outlet valves, the maximum stress during submergence is 3.7 MPa, representing a 12% reduction in stresses as compared to that for valve configuration C1.

In practice, we should aim to submerge the ring structure ahead of predicted storms. Thus, the submergence tends to be carried out under wave action. Understanding the hydroelastic responses of the ring structures in waves is important for selecting an appropriate valve configuration. Figure 14 presents the maximum von Mises stresses in the ring structure at the nine locations for sea-state conditions S1 and S2. It can be seen that the stress during submergence (i.e., Stages 2, 3, 4) can be significantly higher than the stress in the floating state of the ring structure. The increases in stresses can be up to 100% if configuration C1 is used, and the stress can reach 12.7 MPa which may cause damage (kinks) to the ring structure. Note that for the HDPE PE 100, the permissible stress is 13 MPa, as mentioned in the Norwegian Standard for fish-cage designs [38]. The increase in stresses during the submergence is less significant when the C2 configuration is adopted. For configuration C2, the maximum stress during submergence only reaches 8.5 MPa, representing a reduction of 30% in stresses as compared to the maximum stresses for the case of configuration C1. The increase in the stress during submergence may be caused by bending from combined wave action and non-uniform distribution of filled waters. In order to minimise the probability of the structure being damaged, the submergence process should take place in relatively

calm waves, ahead of predicted storms, and by using at least two inlet valves and two outlet valves for a more even distribution of filled waters.

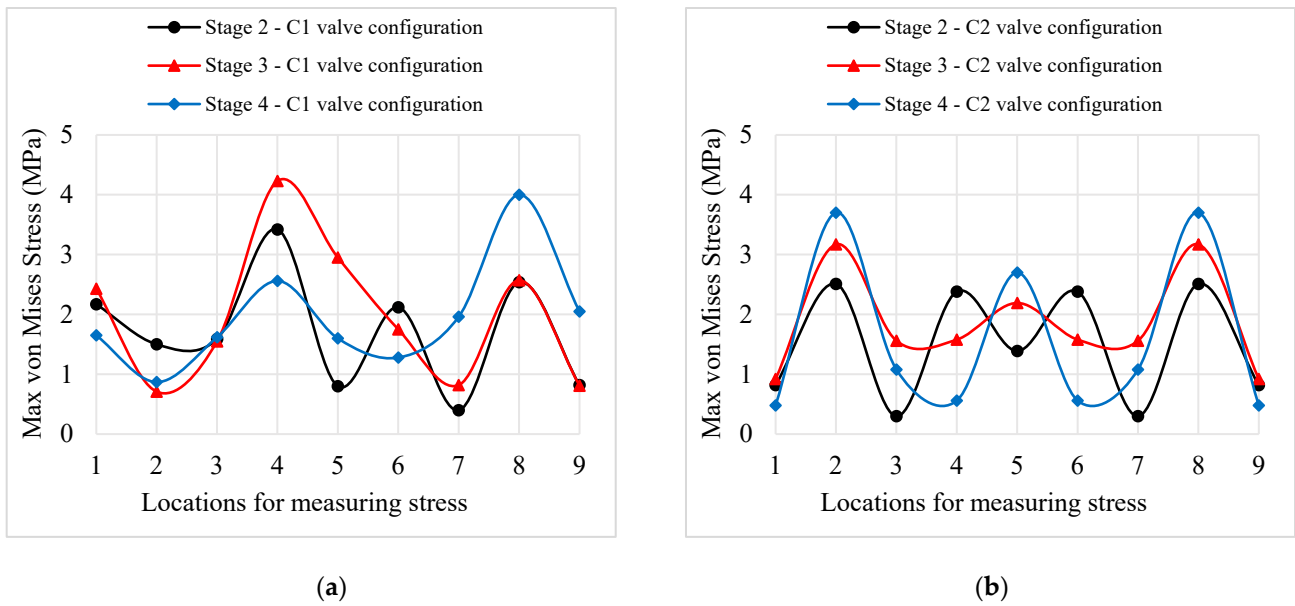


Figure 13. von Mises stresses at various locations of ring structure in calm water: (a) C1 valve configuration, (b) C2 valve configuration.

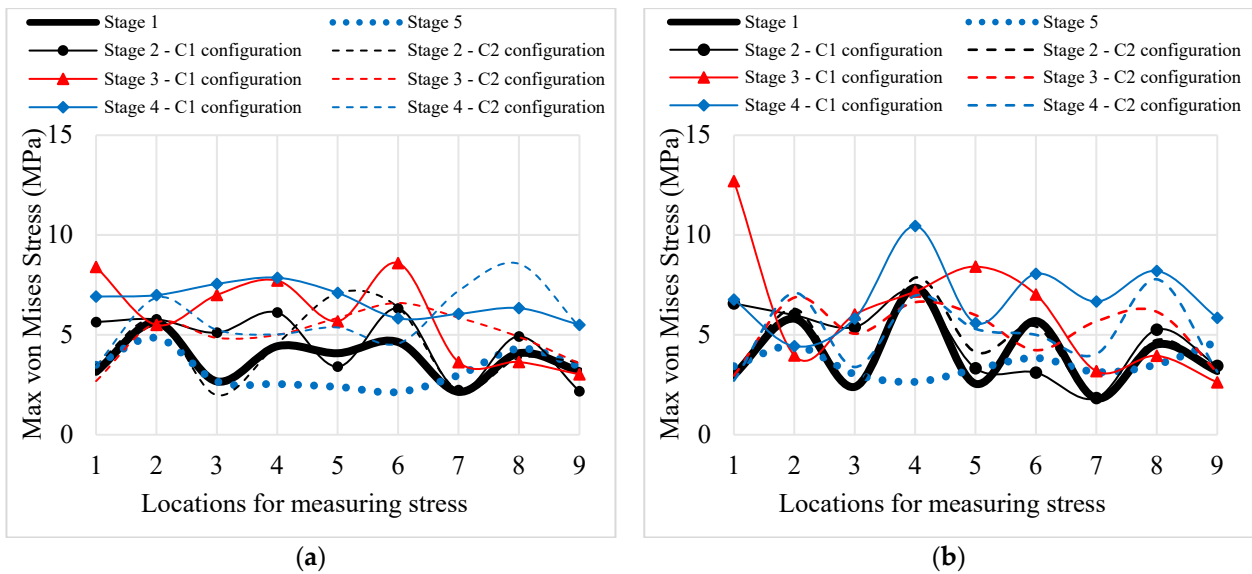


Figure 14. Von Mises stresses at various locations of ring structure under wave action for sea states: (a) S1, (b) S2.

Figure 15 shows the deformed state and stress distributions in the ring structure during submergence (i.e., stages 2, 3, 4) in sea state S2. It can be seen that the stress for the ring structure with valve configuration C2 is lower than that for the ring structure with valve configuration C1. The maximum stresses occur at the connections with bridle lines or at the locations of inlet valves.

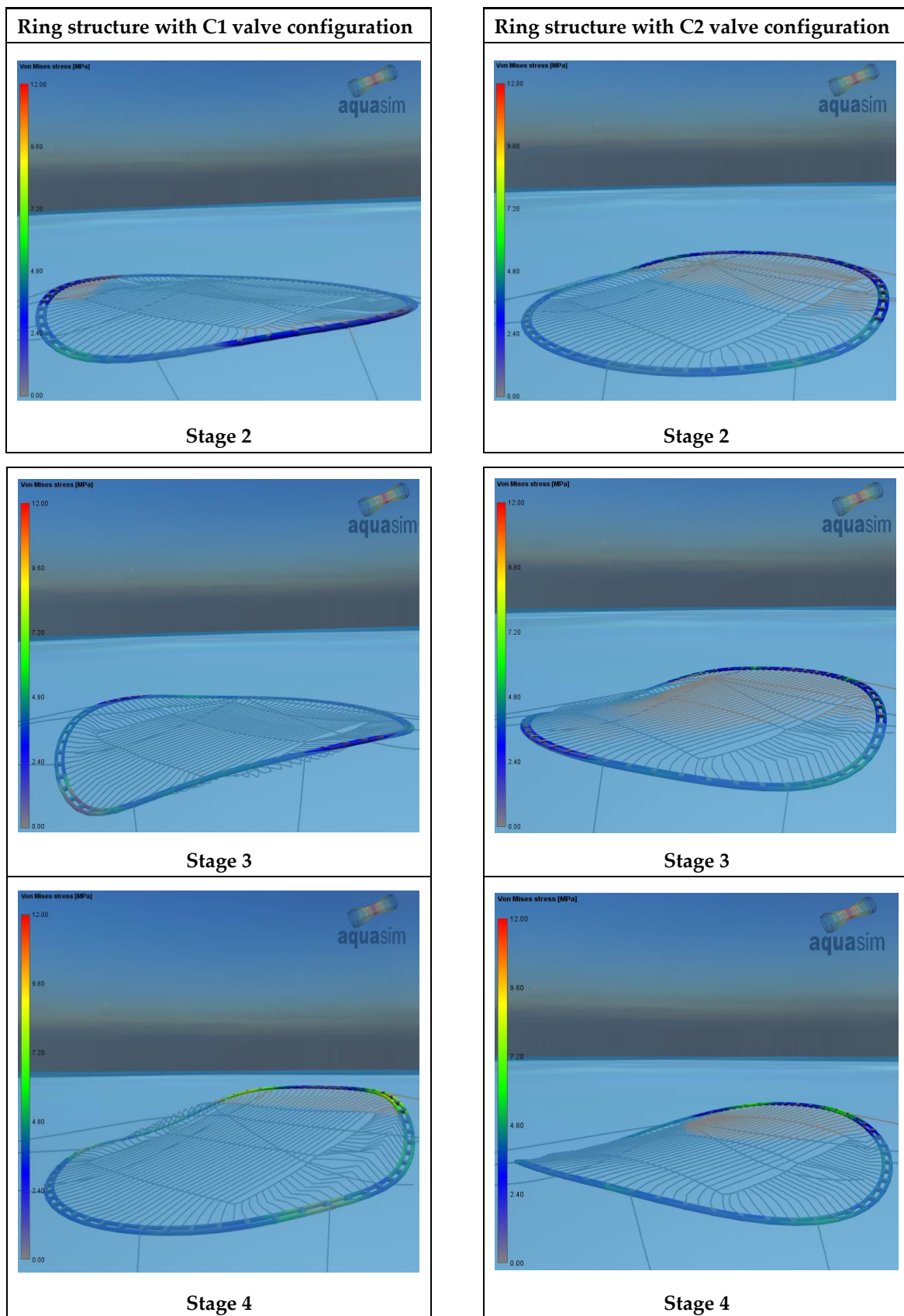


Figure 15. Deformed state and stress distributions in ring structure during submergence for valve configurations C1 and C2 in sea state S2.

5. Concluding Remarks

This paper presents the hydroelastic responses of a submersible ring structure for offshore seaweed cultivation under wave action. The ring structure comprises two circular HDPE pipes connected side-by-side by HDPE brackets. The ring structure carries seaweed grow-out lines, and is kept in position by mooring-line systems commonly used in open-net fish farms. It is designed to have a submersible capability to avoid strong surface waves during storms and can be raised to the surface when the storms end. Submergence is achieved by filling HDPE pipes with water through inlet valves and releasing trapped air through outlet valves. To refloat the ring structure, compressed air is injected into the HDPE pipes through a buoyant inlet valve, allowing the trapped water to be pushed out through the outlet valves. Numerical simulations were made of platforms with one inlet valve and one outlet valve as well as with two inlet valves and two outlet valves in various wave conditions. The following observations are made:

- von Mises stress and mooring forces can be reduced by 50% by submerging the ring structure, thereby increasing the survivability of the seaweed infrastructure in the event of a severe storm;
- von Mises stress may increase during the submergence process. For the ring structure with one inlet valve and one outlet valve, the stress may increase by 100% during submergence as compared to the stress values at the floating stage. However, by using two inlet valves and two outlet valves, the stress can be reduced significantly during submergence. So, it is important to use at least two inlet valves and two outlet valves.

The seaweed-cultivation ring structure examined in this paper can be easily constructed by using available supply chains or by repurposing fish cages with minimal modifications. It can be deployed on the downstream end of fish farms to clean the water as seaweeds soak up excess nitrogen and phosphorus from fish wastes.

Author Contributions: Conceptualization, H.P.N. and C.M.W.; methodology, H.P.N. and C.M.W.; formal analysis, H.P.N., C.M.W. and B.v.H.; writing—original draft preparation, H.P.N. and C.H.; writing—review and editing, C.M.W., B.v.H. and C.H.; funding acquisition, C.M.W. and B.v.H. All authors have read and agreed to the published version of the manuscript.

Funding: This research was funded by the Blue Economy Cooperative Research Centre, established and supported under the Australian Government's Cooperative Research Centres Program, grant number CRC20180101.

Institutional Review Board Statement: Not applicable.

Informed Consent Statement: Not applicable.

Data Availability Statement: The data presented in this study are available from the corresponding author on reasonable request.

Acknowledgments: The authors would like to thank Aquastructures AS for granting access to their software AquaSim.

Conflicts of Interest: The authors declare no conflict of interest. The funders had no role in the design of the study; in the collection, analyses, or interpretation of data; in the writing of the manuscript; or in the decision to publish the results.

References

1. *FAO Seaweeds and Microalgae: An Overview for Unlocking Their Potential in Global Aquaculture Development*; FAO: Québec City, QC, Canada, 2021.
2. Kelly, J. Australian Seaweed Industry Blueprint for Growth. 2020. Available online: <https://www.agrifutures.com.au/wp-content/uploads/2020/09/20-072.pdf> (accessed on 1 November 2023).
3. *FAO Global Seaweeds and Microalgae Production, 1950–2019*; FAO: Québec City, QC, Canada, 2021.
4. Radulovich, R.; Neori, A.; Valderrama, D.; Reddy, C.R.K.; Cronin, H.; Forster, J. Farming of Seaweeds. In *Seaweed Sustainability: Food and Non-Food Applications*; Academic Press: Cambridge, MA, USA, 2015; pp. 27–59. ISBN 9780124199583.
5. Bak, U.G.; Gregersen, Ó.; Infante, J. Technical Challenges for Offshore Cultivation of Kelp Species: Lessons Learned and Future Directions. *Bot. Mar.* **2020**, *63*, 341–353. [CrossRef]

6. Buck, B.H.; Troell, M.F.; Krause, G.; Angel, D.L.; Grote, B.; Chopin, T. State of the Art and Challenges for Offshore Integrated Multi-Trophic Aquaculture (IMTA). *Front. Mar. Sci.* **2018**, *5*, 165. [CrossRef]
7. Tullberg, R.M.; Nguyen, H.P.; Wang, C.M. Review of the Status and Developments in Seaweed Farming Infrastructure. *J. Mar. Sci. Eng.* **2022**, *10*, 1447. [CrossRef]
8. Wang, C.M.; Chu, Y.; Baumeister, J.; Zhang, H.; Jeng, D.-S.; Abdussamie, N. Offshore Fish Farming: Challenges and Developments in Fish Pen Designs. In *Global Blue Economy Analysis, Developments, and Challenges*; CRC Press: Boca Raton, FL, USA, 2022.
9. Tompkins, A.N. Marine Biomass Program Annual Report for 1979. Available online: <https://arpa-e.energy.gov/sites/default/files/1979%20GRI%20Marine%20Biomass%20Program%20Annual%20Report.pdf> (accessed on 1 November 2023).
10. Agency-Energy, T.A.R.P. Macroalgae Research Inspiring Novel Energy Resources. Available online: <https://arpa-e.energy.gov/technologies/programs/mariner> (accessed on 31 January 2022).
11. UNITED. Available online: <https://www.h2020united.eu/> (accessed on 1 November 2023).
12. Fredriksson, D.W.; Dewhurst, T.; Drach, A.; Beaver, W.; St Gelais, A.T.; Johndrow, K.; Costa-Pierce, B.A. Hydrodynamic Characteristics of a Full-Scale Kelp Model for Aquaculture Applications. *Aquac. Eng.* **2020**, *90*, 102086. [CrossRef]
13. Zhu, L.; Lei, J.; Huguenard, K.; Fredriksson, D.W. Wave Attenuation by Suspended Canopies with Cultivated Kelp (*Saccharina latissima*). *Coast. Eng.* **2021**, *168*, 103947. [CrossRef]
14. Nguyen, H.P.; Wang, C.M.; Tullberg, R.; Zhang, X.; von Herzen, B. Hydroelastic Analysis of Submersible Circular Seaweed Platform. In Proceedings of the ASME 2023 42nd International Conference on Ocean, Offshore and Arctic Engineering OMAE2023, Melbourne, Australia, 11–16 June 2023.
15. Watanabe, E.; Utsunomiya, T.; Wang, C.M. Hydroelastic Analysis of Pontoon-Type VLFS: A Literature Survey. *Eng. Struct.* **2004**, *26*, 245–256. [CrossRef]
16. Tay, Z.Y. Energy Extraction from an Articulated Plate Anti-Motion Device of a Very Large Floating Structure under Irregular Waves. *Renew. Energy* **2019**, *130*, 206–222. [CrossRef]
17. Tay, Z.Y. Artificial Neural Network Framework for Prediction of Hydroelastic Response of Very Large Floating Structure. *Appl. Ocean Res.* **2023**, *139*, 103701. [CrossRef]
18. Fu, S.; Moan, T. Dynamic Analyses of Floating Fish Cage Collars in Waves. *Aquac. Eng.* **2012**, *47*, 7–15. [CrossRef]
19. Li, L.; Fu, S.; Xu, Y.; Wang, J.; Yang, J. Dynamic Responses of Floating Fish Cage in Waves and Current. *Ocean Eng.* **2013**, *72*, 297–303. [CrossRef]
20. Liu, H.Y.; Huang, X.H.; Pang, G.L.; Yuan, T.P.; Hu, Y.; Yuan, S. Structural Mechanical Properties of Circular Fish Cages Determined by Finite Element Analysis and Material Test. *Ocean Eng.* **2022**, *261*, 112083. [CrossRef]
21. Dai, J.; Wang, C.M.; Utsunomiya, T.; Duan, W. Review of Recent Research and Developments on Floating Breakwaters. *Ocean Eng.* **2018**, *158*, 132–151. [CrossRef]
22. Chu, Y.I.; Wang, C.M.; Park, J.C.; Lader, P.F. Review of Cage and Containment Tank Designs for Offshore Fish Farming. *Aquaculture* **2020**, *519*, 734928. [CrossRef]
23. Bluegreen, Marine Donut. Available online: <https://bluegreengroup.no/en/services/marine-donut> (accessed on 15 November 2023).
24. Wang, C.-M.; Chu, Y.-I.; Baumeister, J.; Zhang, H.; Qiao, Y.-P.; Karampour, H.; Jeng, D.-S.; Savage, L. SeaFisher—A Submersible High-Density Polyethylene Offshore Fish Pen. *J. Mar. Sci. Eng.* **2023**, *11*, 1795. [CrossRef]
25. Shah, Y.; Yadav, A.; Kumar, M.A.; Kavale, M.G.; Prasad, K.; Mantri, V.A. ‘Proof of Concept’ of How Tube-Net Diameter Affects Growth and Agar Content in Industrially Important Farmed Red Seaweed *Gracilaria Dura*. *J. Appl. Phycol.* **2021**, *33*, 2349–2358. [CrossRef]
26. FAO. Manual of Running Water Fish Culture. Available online: <https://www.fao.org/3/ac416e/AC416E00.htm#ch1.1> (accessed on 1 November 2023).
27. Badinotti Cage Farming Equipment: Submersible and Floating Cages. 2018. Available online: https://www.badinotti.com/wp-content/uploads/2018/03/CAGE-FARMING-EQUIPMENT_PRESS.pdf (accessed on 1 November 2023).
28. Rozvany, G.I.N.; Wang, C.M.; Dow, M. Prager-Structures: Archgrids and Cable Networks of Optimal Layout. *Comput. Methods Appl. Mech. Eng.* **1982**, *31*, 91–113. [CrossRef]
29. Barltrop, N.D.P. *Floating Structures: A Guide for Design and Analysis*; University of Strathclyde: Glasgow, UK, 1988; Volume 2.
30. ScaleAQ, Mooring System. Available online: <https://scaleaq.com/product-category/pen-net-and-mooring/mooring-systems/> (accessed on 1 November 2023).
31. Shen, Y.; Greco, M.; Faltinsen, O.M.; Nygaard, I. Numerical and Experimental Investigations on Mooring Loads of a Marine Fish Farm in Waves and Current. *J. Fluids Struct.* **2018**, *79*, 115–136. [CrossRef]
32. Aquastructures. Aquasim. Available online: <https://aquasim.no/aquasim/history.html> (accessed on 1 November 2023).
33. Jaikumar, M.; Dineshram, R.; Imchen, T.; Mandal, S.; Rangesh, K. Seaweed Farming Potential in India. In *Global Blue Economy*; CRC Press: Boca Raton, FL, USA; Taylor & Francis: Abingdon, UK, 2022; pp. 449–470.
34. Qiao, D.; Mackay, E.; Yan, J.; Feng, C.; Li, B.; Feichtner, A.; Ning, D.; Johanning, L. Numerical Simulation with a Macroscopic CFD Method and Experimental Analysis of Wave Interaction with Fixed Porous Cylinder Structures. *Mar. Struct.* **2021**, *80*, 103096. [CrossRef]
35. Zhao, F.; Kinoshita, T.; Bao, W.; Itakura, H. Theoretical and Experimental Study on a Porous Cylinder Floating in Waves. In Proceedings of the 28th International Conference on Ocean, Offshore and Arctic Engineering, Honolulu, HI, USA, 31 May –5 June 2009; Volume 4, pp. 1261–1268. [CrossRef]

36. FAO Gracilaria Culture in China. Available online: <https://www.fao.org/3/AC263E/AC263E00.htm#:~:text=2.3.-,1Specificgravityofseawater> (accessed on 1 November 2023).
37. Aquatec Offshore Submersible Cage. Available online: <https://aquatecindonesia.com/product/offshore-submersible-cage/> (accessed on 1 November 2023).
38. *NS 9415*; Marine Fish Farms Requirement for Site Survey, Risk Analyses, Design, Dimensioning, Production, Installation and Operation. Norwegian Standard: Oslo, Norway, 2009.

Disclaimer/Publisher's Note: The statements, opinions and data contained in all publications are solely those of the individual author(s) and contributor(s) and not of MDPI and/or the editor(s). MDPI and/or the editor(s) disclaim responsibility for any injury to people or property resulting from any ideas, methods, instructions or products referred to in the content.